Organic & Biomolecular Chemistry

Accepted Manuscript

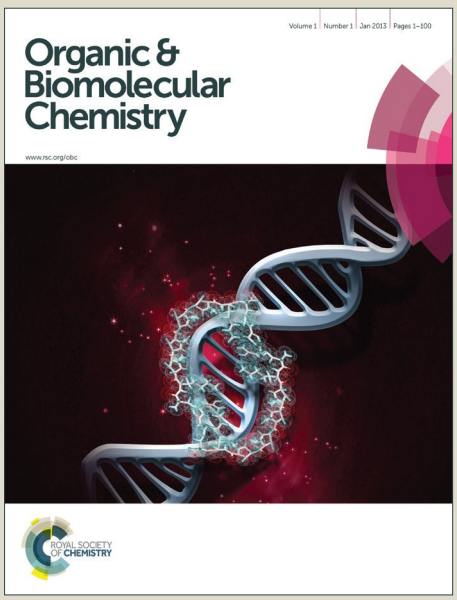

ROYAL SOCIETY OF CHEMISTRY

www.rsc.org/obc

Mechanisms and stereoselectivities of Rh(I)-catalyzed carbenoid carbon insertion reaction of benzocyclobutenol with diazoester

Yanyan Wang, Yang Wang, Wenjing Zhang, Yanyan Zhu, Donghui Wei*, Mingsheng Tang*

College of Chemistry and Molecular Engineering, Center of Computational Chemistry, Zhengzhou University, Zhengzhou, Henan, 450001, PR China

Abstract

In this paper, density functional theory (DFT) study has been carried out to investigate the mechanisms of Rh(I)-catalyzed carbenoid carbon insertion into C–C bond reaction between benzocyclobutenol (**R1**) and diazoester (**R2**). The calculated results indicate that the reaction proceeds through five stages: deprotonation of **R1**, cleavage of C–C bond, carbenoid carbon insertion, intramolecular aldol reaction, and protonation of alkoxyl-Rh(I) intermediate. We have suggested and studied two possible pathways according to different coordination patterns (including ketone-type and enol-type coordination forms) in the fourth stage, and found that the enol-type pathway is favorable, making the coordination mode of Rh(I) center in oxa-π-allyl Rh(I) intermediate clear in this reaction system. Moreover, four possible protonation channels have been calculated in the fifth stage, and the computational results show that the H_2O-assisted proton transfer channel is most favorable. The first step of the third stage is rate-determining, and the first steps in stages 3 and 4 play important roles in determining the stereoselectivities. What's more, the analyses of distortion/interaction, natural bond orbital (NBO), and molecular orbital (MO) have been performed to get better understand on this title reaction. Furthermore, the pathway corresponding to *RR* configurational product is the most favorable path, which is consistent with the experimental result. This work should be helpful for understanding the detailed reaction mechanism and the origin of stereoselectivities of the title reaction, and thus could provide valuable insights on rational design of more efficient catalysts for this kind of reactions.

* E-mail: donghuiwei@zzu.edu.cn
* E-mail: mstang@zzu.edu.cn

Keywords: DFT, Rh(I)-catalyst, Carbenoid Carbon Insertion, Carbon-carbon Cleavage

1. Introduction

Carbon-carbon bond is the most fundamental framework in organic and natural compounds. The C–C bonds activation[1] and subsequent functionalization (called as "cut-and-sew" protocols[2]) are always the most challenging issues in organic chemistry due to the kinetically inert and thermodynamically stable property of C–C bonds.[3] In the "cut" stage, it is an interesting research area in controlling the break of C–C bond selectively, and the following construction of new C–C bonds skeleton is also an attractive point in organic synthesis.

To date, the strained systems such as three- or four-membered cycles activated by strong electron-withdrawing groups or catalyzed by transition-metal catalysts have been widely used[1d, 4] in the "cut" stage, and the unsaturated bonds (i.e. alkenes,[5] alkynes,[2c, 5c, 5d, 6] and carbon monoxide[6-7]) are generally employed as coupling partners to construct new C–C bond framework for the subsequent functionalization. In recent years, the transition-metal-catalyzed selective C–C insertions have attracted more and more attention of both experimental and theoretical chemists.[8] In particular, Murakami's group has recently reported rhodium-catalyzed ring opening of benzocyclobutenols with site-selectivity complementary to thermal ring opening,[9] and the overall transformation is a formal two-carbon insertion reaction. In theory, Morokuma and co-workers[8e] systematically studied the C–C bond activation in Rh-catalyzed ring opening of benzocyclobutenol using the density functional theory (DFT) method. Nonetheless, they only evaluated the Rh(I)-catalyzed site-selectivity of C–C bonds cleavage of benzocyclobutenol, the subsequent functionalization was not studied. Lin's group[8f] investigated the subsequent functionalization, achieving two-carbon (alkyne) insertion reaction. Both of the two groups were focus on the site-selectivity of C–C bonds cleavage of benzocyclobutenol, however, the stereoisomeric channels of this kind of reactions have not been considered in theory before.

More recently, the C–C bonds cleavage along with the one-carbon (carbenoid

carbon) insertion reactions, in which diazo compounds and N-tosylhydrazones[8b, 8c] have been correspondingly employed as the carbene precursors, have emerged as a new class of cross-coupling reaction. For example, Wang et al.[10] reported the first example of Rh(I)-catalyzed formal one-carbon (carbenoid carbon) insertion to afford the indanol products in good yields and excellent stereoselectivity (eq 1, **Scheme** 1), and only one isomer was observed. Subsequently, Murakami[11] reported an enantioselective insertion reaction of a carbenoid carbon into a C–C bond to expand cyclobutanols to cyclopentanols (eq 2, **Scheme 1**), which also achieved the one-carbon (carbenoid carbon) insertion. In these reactions, the diazo compound was employed as carbene precursor to insert into C–C bond of four-membered ring (**Scheme 1**).

Regarding to the reaction mechanism, Wang and co-workers have given a proposal for eq 1 in **Scheme 1**. As depicted in **Scheme 2**, there are five processes in the reaction, including selective cleavage of C–C bond,[8e, 8f, 9] nitrogen dissociation,[12] carbenoid carbon insertion,[8d, 13] intramolecular aldol reaction,[14] and protonation. Nevertheless, it is still difficult to get thorough understanding about mechanism of this kind of Rh(I)-catalyzed reactions unless we can obtain more details at the molecular level. For instance: (1) As shown in **Scheme 2**, the coordination mode of Rh(I) center in oxa-π-allyl Rh(I) intermediate **D** is unclear. (2) Generally, the protic media (such as water) can assist the proton transfer process in many organic reactions and effectively lower the energy barrier. The previous studies of our group[15] also indicated that the bimolecular proton transfer pathway is more beneficial than the direct proton transfer pathway in some reactions, thus we think it is necessary to explore multiple possible proton transfer pathways for the last protonation process. (3) Besides the mechanism, it is important to examine which step is stereoselectivity-determining and what factors control the stereoselectivities of the reaction. All the puzzles mentioned above prompt us to carry out a theoretical investigation towards the mechanisms and stereoselectivities of the title catalytic reaction in-depth and try to make those questions clear.

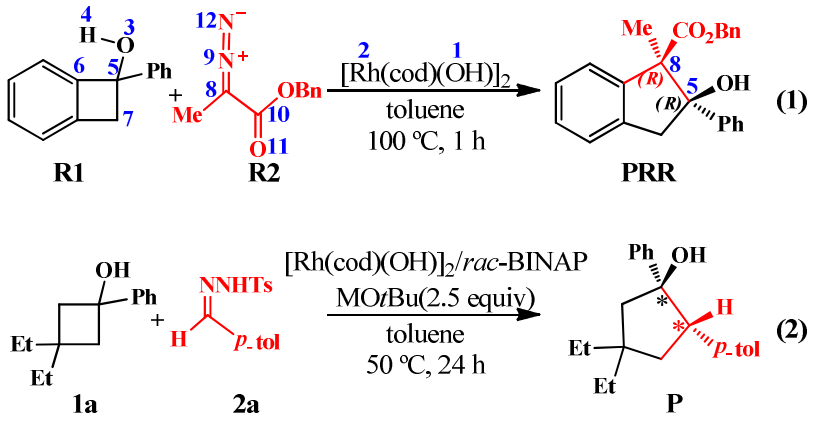

Scheme 1 Rh(I)-catalyzed carbenoid carbon insertion reaction

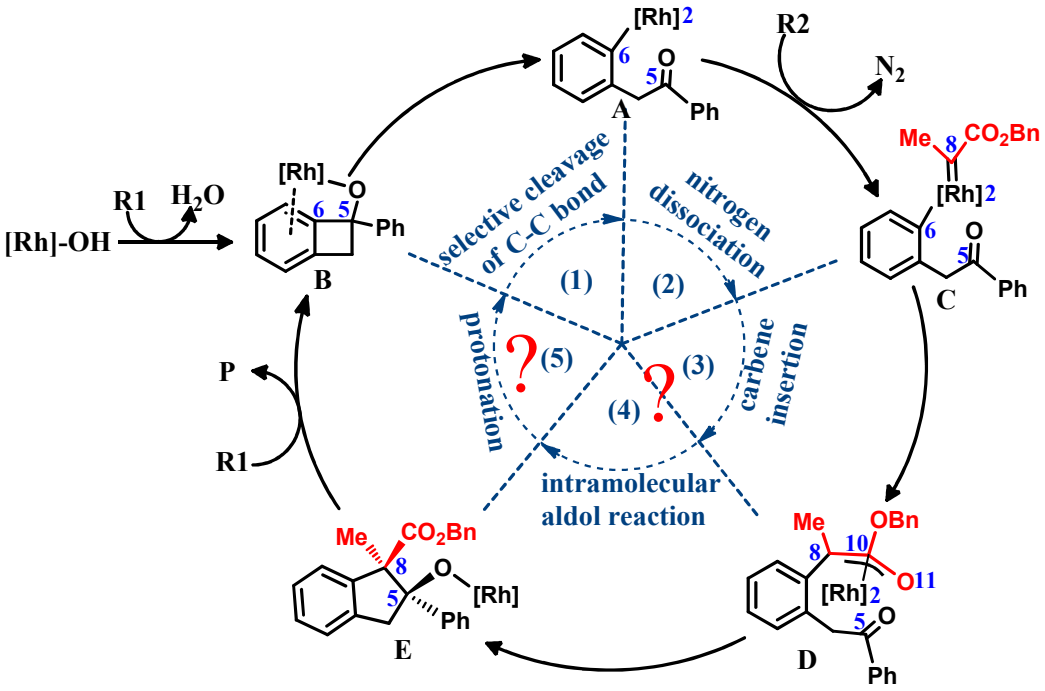

Scheme 2 Proposed mechanism by Wang's group

On base of proposed mechanism of Wang and co-workers, we choose to give a more detailed theoretical study on mechanism and stereoselectivities towards reaction of eq 1 in **Scheme 1**. The density functional theory (DFT) method was applied since it has been successfully used in the studies of organocatalysis,[16] organometallic catalysis[17] and biological reaction mechanisms.[18] For the sake of convenience, the reaction between 1-ph-benzocyclobutenol (denoted as **R1**, **Scheme 1**) and 2-diazobenzylpropanoate (denoted as **R2**, **Scheme 1**) catalyzed by $[Rh(cod)OH]_2$

(**Scheme 1**) has been chosen as the object of investigation. As shown in **Scheme 1**, it should be noted that there are two chiral centers (C5 and C8 atoms) in the final product, and in this paper, we will use the first 'R' or 'S' to represent the chirality of C5 atom, and the second one to represent the chirality of C8 atom.

2. Computational Details

All theoretical calculations were carried out using the *Gaussian 09* program.[19] Geometry optimizations have been performed at the B3LYP[20]/6-31G(d)//LanL2DZ level of theory, in particular, the effective core potentials (ECPs) of Hay and Wadt with a double-ζ valence basis set (LanL2DZ) were used for Rh, and the 6-31G(d) basis set was used for all the other atoms. The solvent effect of toluene was taken into account for all calculations (optimization and frequency) by the self-consistent reaction field (SCRF) method, which is based on the conductor polarizable continuum model (CPCM).[21] Frequency calculations were carried out at the same level to confirm the characteristics of all of the optimized structures as minima (no imaginary frequency) or transition states (one and only one imaginary frequency). The same level of intrinsic reaction coordinate (IRC)[22] calculation was also carried out to verify that the transition state connects correctly to expect local minima. Most significant structures had been represented in the figures by using CYLView.[23]

All energies discussed in this paper are Gibbs free energies rather than Born-Oppenheimer energies, because Gibbs free energies include zero-point energy (ZPE), thermal correction to the electronic (including nuclear-repulsion) energies, and also the entropic factor, but the Born-Oppenheimer energies are only the electronic (including nuclear-repulsion) energies plus the zero-point energy (ZPE) corrections.

To check whether the aforementioned calculation methods can obtain reliable results, we also performed single-point energy CPCM calculations for the key transition states **Re_TS4** and **Si_TS4** involved in the third stage using different functionals at different levels based on the optimized geometries at the B3LYP/6-31G(d)//LanL2DZ level, and the results were shown as Table S1 in Electronic Supplementary Information (ESI). It is easy to see that the differences

between results calculated by those methods and those by aforementioned method (i.e. B3LYP/6-31G(d)//LanL2DZ) are no more than 1.0 kcal/mol. Therefore, we think the level of theory we used is reliable for the systems studied in this work.

To cast light on the factors influencing the key step, we have performed distortion/interaction analysis[24] developed by Houk and co-workers, which provides a highly insightful method for understanding reactivity and activation barriers. In this theory, the activation energy ($\Delta E^{\neq}$) is divided into two main components: the distortion ($\Delta E^{\neq}_{\text{dist}}$) and interaction ($\Delta E^{\neq}_{\text{int}}$) energies. The distortion energy involves geometric and electronic changes to deform the reactants to their transition state geometry.[16a] The interaction energy is obtained by the relationship: $\Delta E^{\neq}_{\text{int}} = \Delta E^{\neq} - \Delta E^{\neq}_{\text{dist}}$.

3. Results and Discussion

At first, it is crucial to determine the real active catalyst for the Rh-complex catalyst. Based on the general study[25] of a related dimeric Rh-catalyzed reaction, the initial dimeric $[Rh(cod)(OH)]_2$ would convertto the monomer Rh(cod)(OH), which has been assumed to be the plausible active catalyst,[8e, 8f] because there is a coordinatively unsaturated rhodium center in the monomer. In this work, we mainly focus on the detailed mechanism and stereoselectivities for the title reaction catalyzed by the plausible active catalyst Rh(cod)(OH) (denoted as **Cat**), which has been depicted in **Scheme 3**.

As can be seen in **Scheme 3**, the fundamental catalytic reaction cycle catalyzed by **Cat** includes five stages, i.e. (1) The complexation process of **R1** and **Cat** for the formation of Rh-alkoxyl complex **M2** along with the proton transfer via transition state **TS1**, and the dehydration via transition state **TS2**. (2) The cleavage of C5–C6 bond to afford intermediate **M3** via transition state **TS3**. (3) The one-carbon (carbenoid carbon) insertion to form the intermediate **M5** via transition states **TS4** and **TS5**, along with the loss of nitrogen and the generation of chiral center C8. (4) The intramolecular aldol reaction (one possible path is the enol-type mechanism (Path A), the other possible path is the ketone-type mechanism (Path B)), accompanied with the

formation of the other chiral center (C5 atom). (5) The protonation of **M7** to form product **P** and the regeneration of the active species. The free energy profiles of the entire catalytic reaction are depicted in **Fig.1** and **Fig.S1** of ESI. The free energies of **R1+R2+Cat** were set as 0.00 kcal/mol as reference. The detailed mechanisms have been discussed stage by stage as follows.

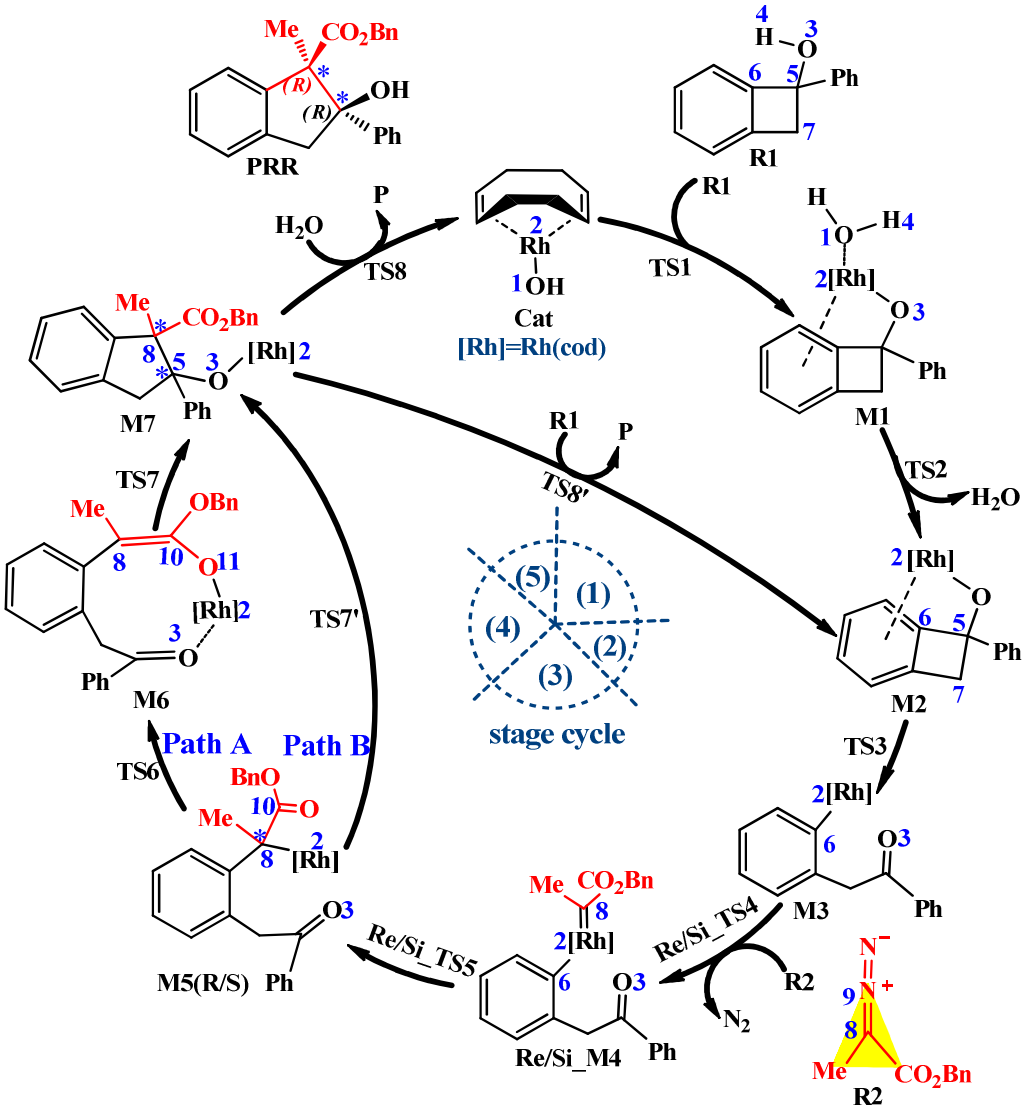

Scheme 3 Possible catalytic cycle of the title reaction

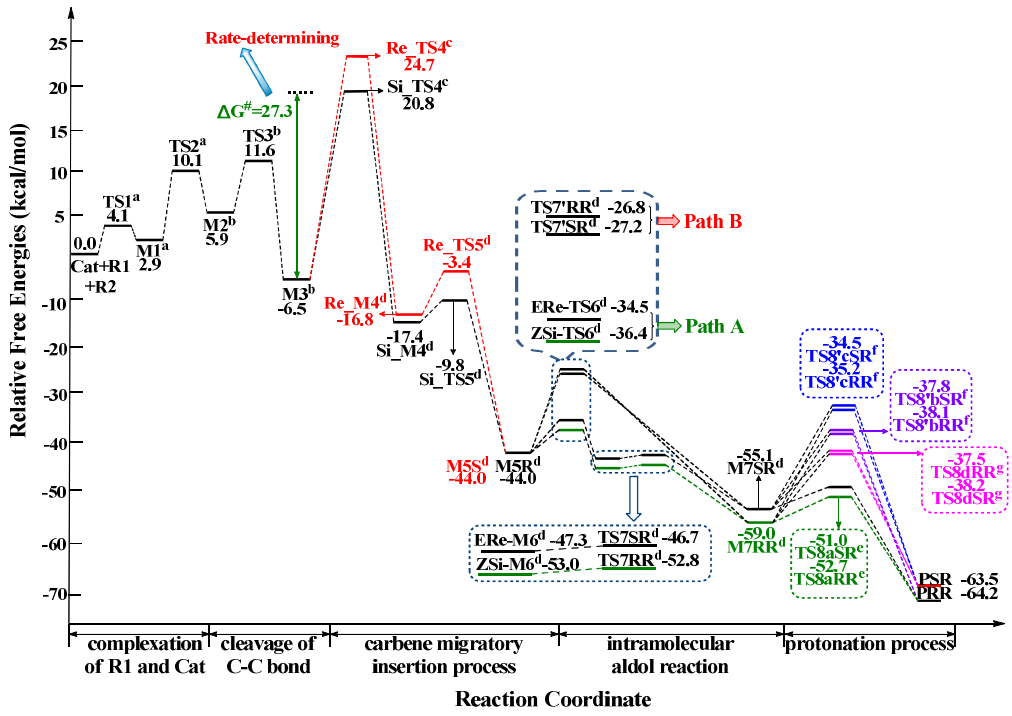

Fig.1 Free energy profiles of the whole catalytic cycle (unit: kcal/mol, the superscripts "a ~ g" represent adding the energy of **R2**, H_2O plus **R2**, H_2O, H_2O plus N_2, N_2, N_2 minus **R1**, N_2 minus **R1** plus H_2O, respectively.

3.1. First stage: the complexation of R1 and Cat

Firstly, **R1** reacts with **Cat** to form intermediate **M1**, which is accompanied with a proton transfer. As shown in **Scheme 3**, the coordinatively unsaturated rhodium center Rh2 of **Cat** would facilely accept the lone pair electrons from O3 atom of benzocyclobutenol **R1** to form intermediate **M1** via transition state **TS1**. **Fig.2** shows the optimized structures involved in the first, second and third stages. The distance between the Rh2 and O3 atoms is shortened from 2.19 Å in **TS1** to 2.07 Å in **M1**, indicating the almost formation of the Rh2–O3 bond in this stage. At the same time, the proton H4 transfers from atom O3 to atom O1 directly via transition state **TS1**. The complexation of **R1** with **Cat** costs only 4.1 kcal/mol in free energy, demonstrating that this step can occur easily under the experimental condition.

Subsequently, the alkoxyl Rh(I) intermediate **M2** is formed by the dehydration of intermediate **M1** via transition state **TS2** (**Scheme 3**), and the free energy barrier for

this step is only 7.2 kcal/mol.

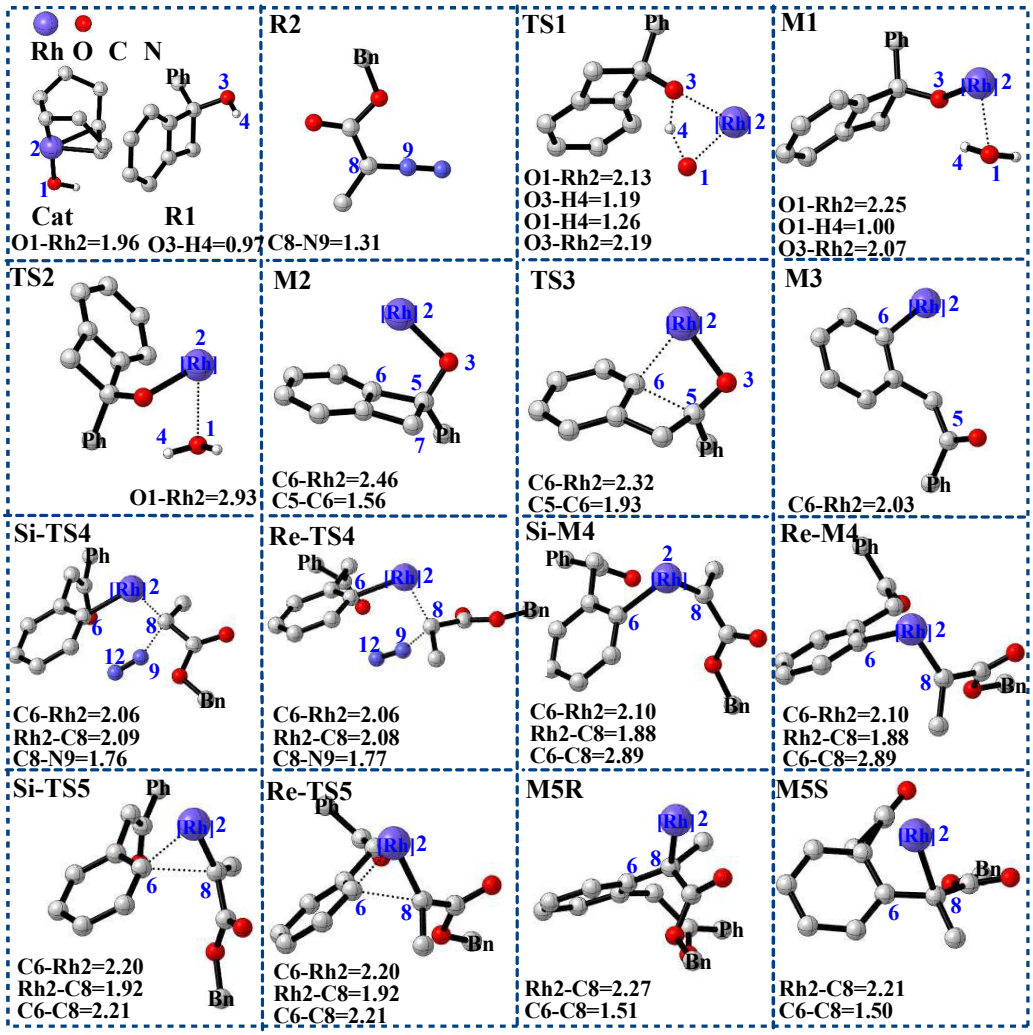

Fig.2 Optimized geometries of the stationary points involved in the first, second, and third stages (the hydrogen atoms and the ligand of Rh(I) which are not involved in the reaction are omitted; only the α-carbon of phenyl and benzyl group are shown; distances in Å).

3.2. Second stage: cleavage of the C5–C6 bond

Noteworthy, Morokuma and co-workers[8e] have systematically studied the $C5_{sp3}$–$C6_{sp2}$ versus $C5_{sp3}$–$C7_{sp3}$ site selectivity in the C–C bond activation in Rh-catalyzed ring opening of benzocyclobutenol using DFT method. They found the $C5_{sp3}$–$C6_{sp2}$ cleavage is favored over the $C5_{sp3}$–$C7_{sp3}$ cleavage. Based on their study, we only consider the favorable $C5_{sp3}$–$C6_{sp2}$ cleavage pathway in this stage.

The second stage is the selective cleavage of C5–C6 bond concerted with the formation of Rh2–C6 bond to generate the intermediate **M3** via transition state **TS3**. The distance changes of C5–C6 and C6–Rh2 in intermediate **M2** (1.56 Å and 2.46 Å respectively, **Fig.2**) to those in transition state **TS3** (1.93 Å and 2.32 Å respectively, **Fig.2**) indicate the gradual cleavage of C5–C6 bond and the gradual formation of C6–Rh2 bond. As shown in **Fig.1**, the free energy barrier of this stage is 5.7 kcal/mol, which is nearly identical with results reported by Morokuma and Lin,[8e, 8f] and it is obvious that this stage is a facile process under the experimental condition.[10]

In order to get better understand about factors leading to the low free energy of activating C5–C6 bond in **M2,** we have performed the analysis of molecular orbitals (MOs) of **M2**. As can be seen in **Fig.3**, **Fig.S2** and **Table 1** obviously, there is an interaction between the *d* orbital of Rh and the π orbital of benzene ring in **M2**, in other words, here the benzene ring acts as a ligand of Rh, so there should be an electron transfer from the benzene ligand to Rh, which has been proved by AIM[26] and NBO analyses (see ESI). This electron transfer leads to the C5–C6 bond becoming weaker in **M2** than that in **R1**, which can be verified by the elongation of C5–C6 bond from 1.54 Å in **R1** to 1.56 Å in **M2**. So we consider this *d*-π interaction would be responsible for the low free energy (5.7 kcal/mol) of activating C5–C6 bond in **M2**.

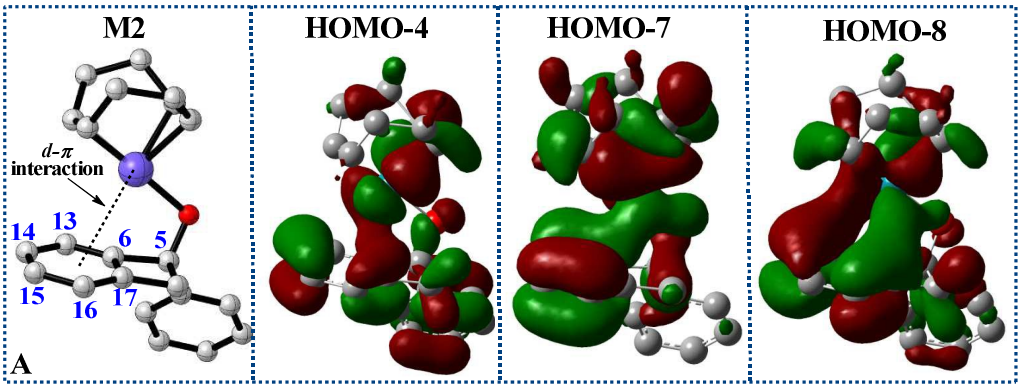

Fig.3 Molecular orbitals of intermediate **M2** (Please refer to **A** for the molecular orientation of the right three MOs).

Table 1 Atomic orbital contributions to molecular orbitals of **M2**

Molecular orbitals	Atomic orbital contributions[a]						
	Rh2	C6	C13	C14	C15	C16	C17
HOMO-4	0.41	--	--	0.09	--	--	0.08
HOMO-7	0.13	0.08	0.11	--	0.08	0.11	--
HOMO-8	0.23	--	0.11	0.17	--	0.09	0.15

Note: [a]The minimum contribution percentage for inclusion in individual orbital population analysis is selected as 8.

3.3. Third stage: the carbenoid carbon migratory insertion process

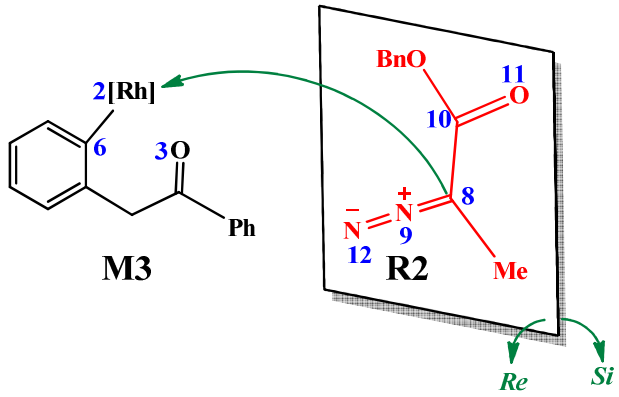

Scheme 4 Illustration of the stereochemistry in the first step of the third stage

The third stage includes two steps: formation of rhodium carbene and carbene migratory insertion. In particular, in the first step, reactant **R2** is attacked by intermediate **M3** for the formation of rhodium-carbene intermediate **M4**, which is concerted with the loss of nitrogen. **Scheme 4** illustrates the stereochemistry involved in the first step of the third stage. It is clear that **M3** can attack on either the *Re* or *Si* face of **R2**. As a result, there are two pathways according to the different attack ways in this step. On the basis of their characteristics, it is reasonable to predict that the two reaction pathways should be quite similar.

At first, the *Re/Si* faces of C8 atom in **R2** can attack Rh2 atom of **M3** to form rhodium-carbene intermediates **Re/Si_M4** via transition states **Re/Si_TS4** respectively. As depicted in **Fig.2**, the distance changes of Rh2–C8 and C8–N9 clarify the gradual formation of rhodium-carbene bond, along with the dissociation of nitrogen from diazoester **R2**. Subsequently, in the second step, the formed intermediates **Re/Si_M4** proceed the carbenoid carbon migratory insertion reaction for the formation of intermediates **M5**(**S/R**) via transition states **Re/Si_TS5**, respectively. Taken together, in this whole stage, the different nucleophilic attacks to the prochiral faces of **R2** eventually lead to the chiral carbon center (C8 atom) in intermediates **M5**(**S/R**).

The free energy barriers of the formation of rhodium-carbenoid carbon step are 31.2 and 27.3 kcal/mol for the *Re/Si*-faces attack pathway, respectively. Correspondingly, the one-carbon (carbenoid carbon) migratory insertion process only costs 13.4 and 7.6 kcal/mol for the formation of intermediates **M5**(**S/R**), separately. Obviously, the *Si*-face nucleophilic attack pathway associated with the formation of *R*-configurational intermediate **M5R** is more energetically favorable than the *Re*-face attack pathway.

As shown in **Fig.1** and **Fig.S1**, the formation of rhodium-carbenoid carbon step (i.e. the first step of the third stage) plays an important role in the entire reaction process, which is not only a rate-determining, but also a stereoselectivity-determining step. To cast light on the factors influencing this step, we have performed (1) distortion/interaction,[24] and (2) natural bond orbital (NBO)[27] and frontier molecular orbital (FMO) analyses. Now the detailed discussions one by one are presented as follows: (1) In the present study, each transition state of **Re_TS4** and **Si_TS4** was divided into two fragments (the distorted **R2** and **M3**), and then we performed single-point energy calculations on each fragment. The energy differences between the distorted fragments and the corresponding optimized ground state structures are the distortion energies (i.e. $\Delta E^{\neq}_{\mathrm{dist\_M3}}$ and $\Delta E^{\neq}_{\mathrm{dist\_R2}}$). The total distortion energy ($\Delta E^{\neq}_{\mathrm{dist\_total}}$) is the summary of $\Delta E^{\neq}_{\mathrm{dist\_M3}}$ and $\Delta E^{\neq}_{\mathrm{dist\_R2}}$. As shown in **Table 2**, the total

distortion energy mainly stems from the deformation of **R2**, which is due to the destruction of the conjugated system. Comparing the distortion/interaction energies of these two transition states, we can see the difference of $\Delta E^{\neq}$ (2.58 kcal/mol) via **Si_TS4** and **Re_TS4** mainly comes from the difference of $\Delta E^{\neq}_{\text{dist\_total}}$ (2.17 kcal/mol), especially that of $\Delta E^{\neq}_{\text{dist\_M3}}$ (1.59 kcal/mol). In other words, the $\Delta E^{\neq}_{\text{dist\_M3}}$ via **Si_TS4** is lower than that via **Re_TS4**, which is mainly responsible for the lower activation energy via **Si_TS4**. Further investigation about the distortion of M3-part has been conducted by overlap the M3-parts of **M3**, **Si_TS4** and **Re_TS4**, and the results indicate that the M3-part structure in **Si_TS4** is more condensed than that in **Re_TS4**, demonstrating the intramolecular interaction in **Si_TS4** should be stronger than that in **Re_TS4** (see ESI), so the discussed above would be responsible for the lower distortion energies via **Si_TS4**. (2) The NBO charge and FMO analyses have also been performed, in which we chose the favorable transition state **Si_TS4** as model. The analysis of NBO charge demonstrates that there is a electron transfer of 0.165 e from **R2** to **M3** in this reaction process. As shown in **Fig.4**, the highest occupied molecular orbital (HOMO) of **R2** is bonding between C8 and N9, while antibonding between N9 and N12, so the electron loss of **R2** is in favor of the cleavage of C8–N9 bond and the formation of N9–N12 triple bond.

Table 2 Distortion/interaction analysis for the first step of the third stage

(Unit: kcal/mol)

	$\Delta E^{\neq}_{\text{dist\_M3}}$	$\Delta E^{\neq}_{\text{dist\_R2}}$	$\Delta E^{\neq}_{\text{dist\_total}}$	$\Delta E^{\neq}_{\text{int}}$	$\Delta E^{\neq}$
Re-TS4	5.96	38.53	44.49	29.44	15.05
Si-TS4	4.37	37.95	42.32	29.85	12.47

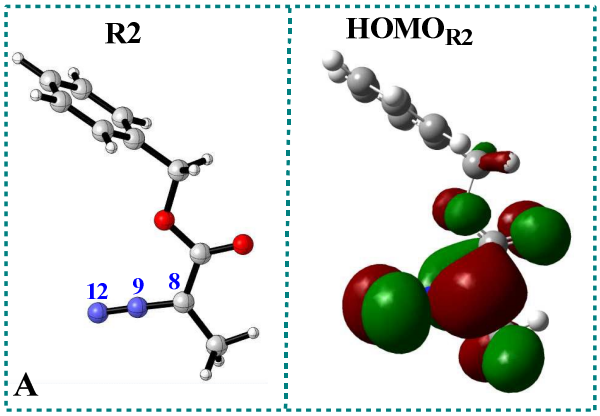

Fig.4 Highest occupied molecular orbital of **R2** (Please refer to **A** for the molecular orientation of the **HOMO$_{R2}$**).

3.4. Fourth stage: the intramolecular aldol reaction

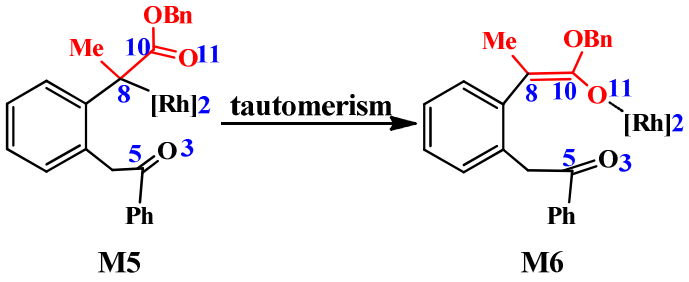

Scheme 5 The tautomerism from **M5** to **M6**

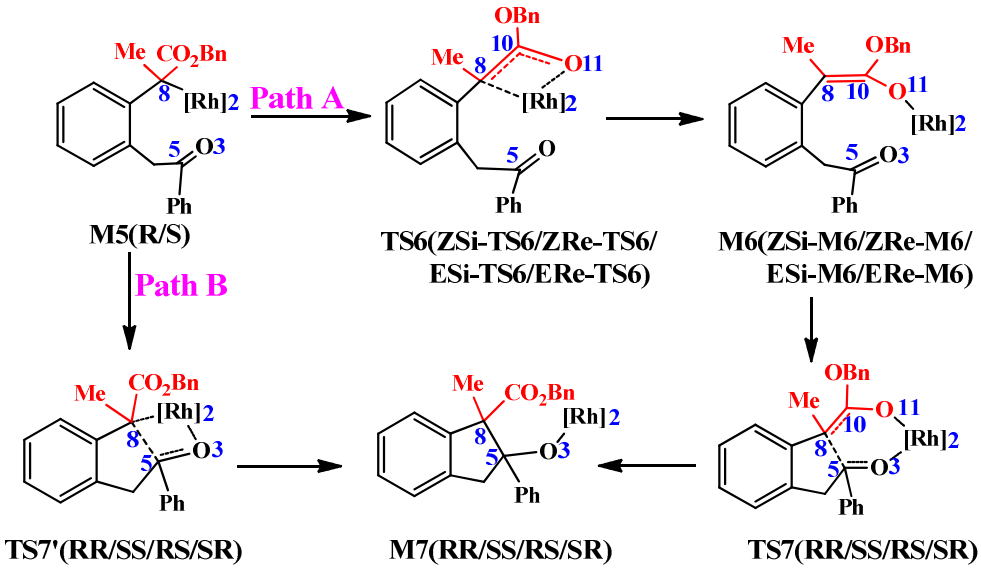

Scheme 6 Possible Reaction Mechanisms for the Fourth Stage

As shown in **Scheme 5**, **M5** could appear as two possible forms (i.e. enol-type and ketone-type) in the course of the tautomeric migration of [Rh] from the adjacent carbon atom C8 to a carbonyl oxygen atom O11, so two possible reaction pathways (Paths A and B, **Scheme 6**) can take place during this stage due to the different coordinative patterns. What's more, according to the different attack modes, there are four modes in each path. Specifically, in Path A, as shown in **Scheme S2**, the intramolecular attack from the C8 atom with *E***-** or *Z***-**isomerism of C8=C10 double bond to the C5 atom with *Re***-** or *Si***-** face of the carbonyl group can afford correspondingly four distereoisomers **M7**(**SR/RS/SS/RR**), respectively; while in Path B, four possible reaction modes should be involved: the C8 atom can attack either the *Re* or *Si* face of the carbonyl group to participate in the intramolecular aldol reaction. The attack on the *Re*- or *Si*-face of the carbonyl group (**Scheme S4**) by the *R*-configuration of the C8 atom can lead to the diastereoisomeric intermediates **M7SR** and **M7RR**, respectively. Whereas the attack on the *Re*- or *Si*-face of the carbonyl group (**Scheme S4**) by the *S*-configuration of the C8 atom can lead to the diastereoisomeric intermediates **M7RS** and **M7SS**, separately. For the convenience of discussion, we have just shown detailed discussions of the most favorable modes in each path as reference. The detailed discussions about the other possible modes are depicted in ESI. In Path A, the suffix "(Z/E)" represents the *cis/trans* isomerism of C8=C10 double bond, respectively.

Enol-Type mechanism (Path A): Scheme 7 illustrates the detailed reaction processes of the most favorable mode for the enol-type aldol reaction pathway, from which we can see the enol-type mechanism includes two steps: tautomerism between **M5** and **M6** (i.e. the first step) and intramolecular aldol-type reaction (i.e. the second step). In the first step, **M5R** could correspondingly convert to **ZSi-M6** via transition states **ZSi-TS6**. The next step is the intramolecular aldol-type reaction of intermediates **ZSi-M6** to form intermediates **M7RR** via transition states **TS7RR**, respectively. The specific attack modes of the transition states **ZSi-TS6** and **TS7RR**

are presented in **Scheme 8**. As shown in **Scheme 8**, the intramolecular attack from the C8 atom with *Z*-isomerism of C8=C10 double bond to the C5 atom with *Re*- face of the carbonyl group can afford correspondinglyisomer **M7RR**. The distance changes of Rh2–O11, Rh2–C8, C10–C8, C8–C5, C5–O3 and O3–Rh2 summarized in **Table S3** (in ESI) and **Fig.4** reveal the gradual accomplishment of this stage.

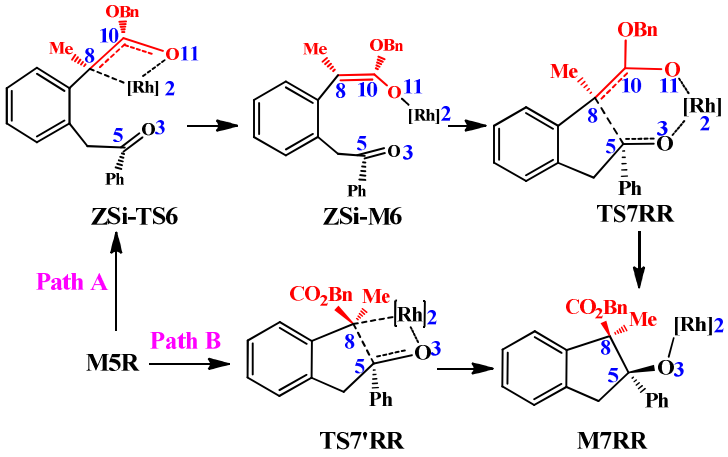

Scheme 7 The most favorable modes in Path A and Path Bin the fourth stage

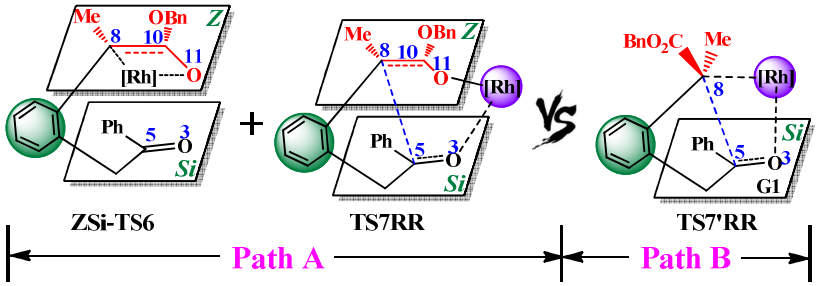

Scheme 8 The most favorable modes for the intramolecular aldol reaction transition states

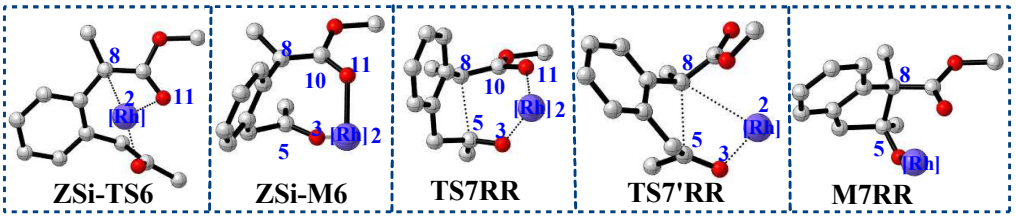

Fig.4 Optimized geometries of the stationary points involved in the most favorable modes in the fourth stage (For parameters of bond lengths, please see Table S2 and S3

in ESI, the hydrogen atoms and the ligand of Rh(I) which are not involved in the reaction are omitted; only the α-carbon of phenyl and benzyl group are shown).

Ketone-Type mechanism (Path B): Scheme 7 depicts the detailed reaction process of the most favorable mode for the ketone-type aldol reaction pathway in the fourth stage, and the most favorable attack faces in **TS7'** are also presented in **Scheme 8**. In this path, the *Si*-face attack on C5 atom of carbonyl group by C8 atom in **M5R**, concerted with the breaking of C8–Rh2 bond leads to isomer **M7RR** via transition state **TS7'RR**.. The distance changes of C5–C8 and C8–Rh2 summarized in **Table S4** (in ESI) and **Fig.4** reveal that the gradual accomplishment of this stage.

It should be noted that **Fig.1** does not show the profiles of the pathways associated with the transformations from **M5S** to its corresponding products **P**(**SS**/**RS**), which can be found in **Fig.S1** in ESI. As shown in **Fig.1** and **Fig.S1**, the energy barriers of the tautomerism step are 9.6 (via **ESi-TS6**), 7.0 (via **ZRe-TS6**), 7.5 (via **ZSi-TS6**) and 9.5 (via **ERe-TS6**) kcal/mol, separately, and those of the following intramolecular aldol-type reaction processes via **TS7RS**, **TS7SR**, **TS7RR**, **TS7SS** are 0.6, 0.6, 0.2, and 0.3 kcal/mol in Path A, separately, while those energy barriers via Path B are 21.8 (via **TS7'RS**), 17.3 (via **TS7'SS**), 17.2 (via **TS7'RR**), 16.8 (via **TS7'SR**) kcal/mol, respectively. Obviously, the enol-type mechanism (Path A) is more energy favorable than the ketone-type mechanism (Path B).

The method of non-covalent interaction (NCI)[28] index developed by Yang and co-workers was demonstrated to be capable of distinguishing strong interaction, Van der waals interaction and repulsive steric interactions. **Fig.5** shows the NCI results for the transition states **TS7RR** (**TS7'RR**) and **TS7SR**, which are the key for the stereoselectivity at the C5 atom. As shown in **Fig.5**, three blue disks (C-O···Rh, C-O···Rh and C=C···C) are found in **TS7RR**, which are indicative of strong attractions. Although these features are also observed in **TS7SR**，there are two unfavorable repulsive steric interactions, which is responsible for the favorability of the *RR* configuration. While in **TS7'RR** of the unfavorable channel, no strong attractions are found, but there are still two weak interactions observed. As concerned above, the

strong intramolecular interactions play important roles in the origin of the stereoselectivity at the C5 atom.

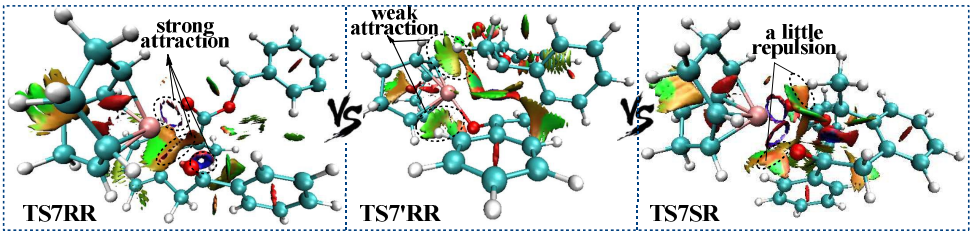

Fig.5 Noncovalent interaction analysis of **TS7RR** ,**TS7'RR, TS7RR** (blue, strong attraction; green, weak interaction; orange, little repulsion)

3.5. Fifth stage: the protonation of M7 to form product and regeneration of catalyst

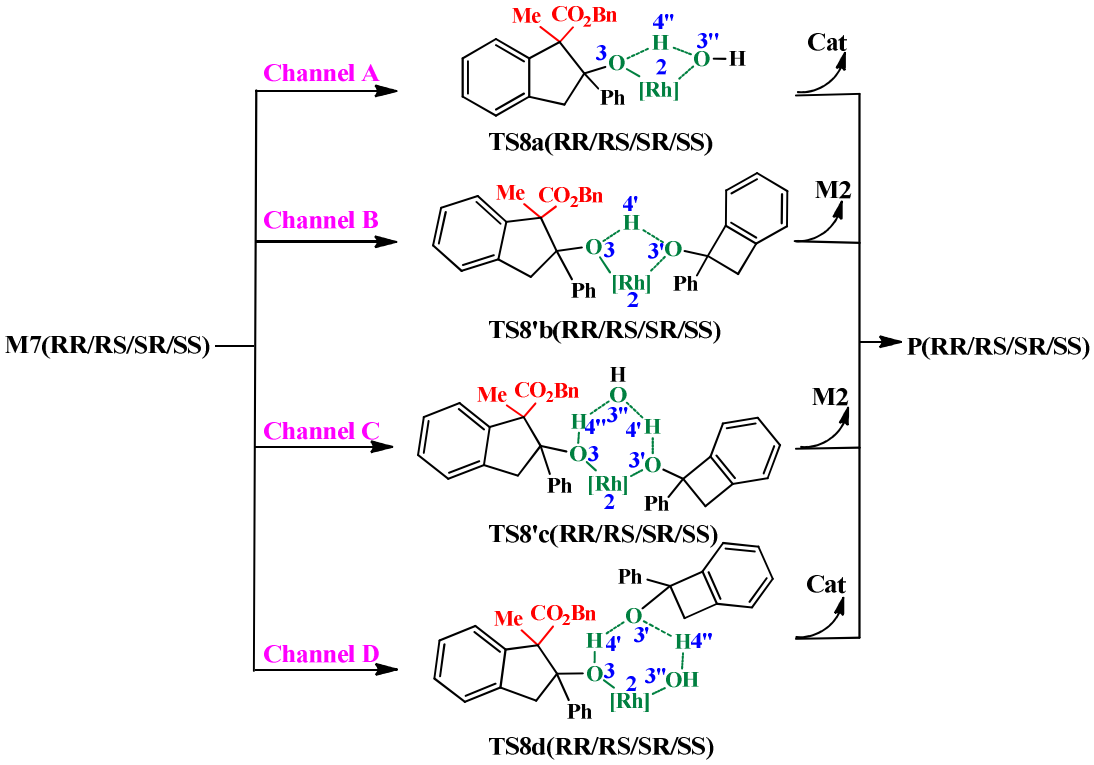

Scheme 11 Possible reaction mechanisms for the fifth stage

The last stage is the protonation of **M7**, which leads to the formation of final products and the regeneration of the Rh-complex catalyst. As depicted in **Scheme 11**, there are four possible channels for the fifth reaction stage: i.e. the H_2O-assisted

protonation channel (Channel A, **Scheme 11**), the **R1**-assisted protonation channel (Channel B, **Scheme 11**), and the bimolecule-assisted (i.e. **R1** and H_2O co-assisted) protonation channels (Channels C and D, **Scheme 11**). It should be noted that there are also four different distereomeric transition states in each channel, so sixteen pathways are considered in this stage. The free energy profiles and optimized structures of all stationary points involved in this stage can be found in **Fig.S1** and **Fig.S2** in ESI. The results of comparing free energy barriers of four channels (**Fig.1** and **Fig.S1**) show that Channel A is the most energy favorable channel, and *RR*-configurational pathway of Channel A is the most energy favorable pathway. Herein, we have only shown detailed discussions of *RR*-configurational distereoisomer in Channel A as reference (discussions about other channels are depicted in ESI).

In Channel A (**Scheme 11**), the proton H4" transfers from O3" to O3 with the help of H_2O, which is concerted with the coordination of O3" and Rh2 atoms and the break of Rh2–O3 bond via the transition states **TS8aRR**. **Fig.S2** in ESI shows that the distances of Rh2–O3, O3–H4", H4"–O3", and O3"–Rh2 in transition states **TS8aRR** are 2.25, 1.22, 1.22, and 2.13 Å, respectively. This indicates that the H_2O-assisted protonation process is in a concerted manner.

3.6. The origin of stereoselectivity

As shown in **Fig.1** and **Fig.S1**, the formation of rhodium-carbenoid carbon step (i.e. the first step of the third stage) should be the rate-determining step, and the activation free energy via transition state **Si_TS4** (corresponding to the formation of **M5R** and **P**(**RR**/**SR**) is 3.9 kcal/mol below that of **Re_TS4** (corresponding to the formation of **M5S** and **P**(**SS**/**RS**)), indicating that the reaction mainly occurs via **M5R** to generate **P**(**RR**/**SR**). Obviously, the free energy barriers of pathway in green color (corresponding to the formation of **PRR**, **Fig.1**) are lower than those in black color (corresponding to the formation of **PSR**, **Fig.1**). So the pathway associated with the formation of **PRR** is the most favorable path, indicating **PRR** rather than **PSR** should be the main product of the reaction, which is in agreement with the experimental

results[10].

As discussed above, the chirality center (C8 atom) forms firstly in the first step of the third stage. Subsequently, the intramolecular enol-type aldol reaction step (i.e. the first step of Path A) forms the other prochirality center (C5 atom) in the fourth stage. So the first step of the third stage and the first step of Path A of the fourth stage are important in controlling the stereoselectivity of this kind of reaction.

3.6.1. Solvent effect on the stereoselectivity

The influence of the DMSO as the solvent was also theoretically considered using CPCM model. The calculated energy difference 3.3 kcal/mol between **Re_TS4** and **Si_TS4** in DMSO is smaller than the difference 3.9 kcal/mol in toluene (see **Table S4**) indicating that using DMSO as solvent in this reaction system can reduce the preference of **Si_TS4**, in other words, the stereoselectivity should become worse. The different change values of **Re_TS4** (8.5 kcal/mol) and **Si_TS4** (8.1 kcal/mol) from toluene to DMSO can be ascribed to their different polarity. The dipole moment of **Re_TS4** is 4.88 D, which is larger than that of **Si_TS4** (2.93 D).

4. Conclusions

In this article, the reaction mechanisms and stereoselectivities of Rh(I)-catalyzed carbenoid carbon insertion into C–C bond reaction of benzocyclobutenol with diazoester have been investigated for the first time using the DFT method. The calculated results indicate that the most favorable reaction pathway contains the following stages: (1) the complexation process of **R1** and **Cat** along with the proton transfer from O3 to O1 atom, and then the elimination of a molecule of H_2O for the formation of Rh-alkoxyl complex **M2**, (2) the cleavage of C5–C6 bond to afford intermediate **M3**, (3) the one-carbon (carbenoid carbon) insertion to form the intermediate **M5**, (4) the tautomerism of **M5** to **M6** and the intramolecular enol-type aldol reaction leading to the intermediate **M7RR**, (5) the H_2O-assisted protonation process for the formation of **PRR** and regeneration of **Cat**. There are two points are

worthy mentioning particularly by the analysis on the calculated results, the one is the coordination mode of Rh(I) center in oxa-π-allyl Rh(I) intermediate in the fourth stage and the other is the way of proton transfer in the fifth stage. Specifically, the enol-type pathway (Path A) is the favorable than ketone-type pathway (Path B) in the fourth stage, that is to say, in this reaction system the Rh(I) center in oxa-π-allyl Rh(I) intermediate is more inclined to the enol-type coordination mode and in the fifth stage, the H_2O-assisted proton transfer channel (Channel A) is the most favorable protonation process. Those results no doubt can offer some ideas for the experimental and theoretical chemists. For instance, it can provide valuable insights to rational design the structure of catalyst to strength the interaction between catalyst and reactant, which is the key for the high stereoselecties of this kind of reactions. Moreover, it also can give a clue/example to predict the stereoselectivity of novel catalytic reaction using NCI and AIM analyses in theory. In addition, the novel, general mechanistic insights obtained in this study should also be helpful for studying/examining possible reaction pathways for other reactions involving such mechanistic question as the enol-type coordination pathway *versus* the ketone-type coordination pathway.

The first step of the third stage (via transition state **Si_TS4**) is the rate-determining step for the entire reaction, and the activation free energies of this step is located at 27.3 kcal/mol, indicating the reaction can proceed smoothly under the experiment condition (100℃). The computational results reveal that the product with *RR* configuration is the major stereoisomer, which is consistent with the experimental results. Notably, the analysis of MO show the *d*-*π* interaction leads to the low free energy barrier (5.7 kcal/mol) of C5–C6 cleavage in the second stage. What's more, the first step of third stage plays an important role in the entire reaction, not only because it is the rate-determining step but also responsible for the generation of the first chiral carbon center C8 atom. The distortion/interaction analysis reveals that the distortion energy of the diazoester part is mainly responsible for the formation of stereoselectivity in this step. Moreover, the NBO and FMO analyses illustrate that

the charge transfer is in favor of the cleavage of C8–N9 bond and the formation of N_2. The first step of the fourth stage (Path A) determines the other stereoselectivity (to form the chiral center C5 atom). The new insights obtained in present study should be useful for the rational design of efficient and highly stereoselective organometal catalytic reactions.

Acknowledgements

The work described in this paper was supported by the National Natural Science Foundation of China (No. 21303167), China Postdoctoral Science Foundation (No. 2013M530340).

References

(1) (a) M. Murakami; H. Amii; Y. Ito, *Nature* **1994**, *370*, 540-541; (b) C. H. Jun, *Chem. Soc. Rev.* **2004**, *33*, 610-618; (c) M. Murakami; M. Makino; S. Ashida; T. Matsuda, *B. Chem. Soc. Jpn.* **2006**, *79*, 1315-1321; (d) G. B. Dong, *Synlett.* **2013**, *24*, 1-5; (e) W. L. Chen; X. Fu; L. L. Lin; X. Yuan; W. W. Luo; J. H. Feng; X. H. Liu; X. M. Feng, *Chem. Commun.* **2014**, *50*, 11480-11483; (f) W. L. Chen; L. L. Lin; Y. F. Cai; Y. Xia; W. D. Cao; X. H. Liu; X. M. Feng, *Chem. Commun.* **2014**, *50*, 2161-2163; (g) S. K. Murphy; J. W. Park; F. A. Cruz; V. M. Dong, *Science* **2015**, *347*, 56-60.

(2) (a) H. M. D. Ko, G., *Nat. Chem.* **2014**, *6*, 739; (b) T. Xu; G. Dong, *Angew. Chem. Int. Ed.* **2012**, *51*, 7567-7571; (c) T. Xu; H. M. Ko; N. A. Savage; G. Dong, *J. Am. Chem. Soc.* **2012**, *134*, 20005-20008; (d) T. Xu; G. Dong, *Angew. Chem. Int. Ed.* **2014**, *53*, 10733-10736; (e) A. Yada; S. Fujita; M. Murakami, *J. Am. Chem. Soc.* **2014**, *136*, 7217-7220.

(3) F. Chen; T. Wang; N. Jiao, *Chem. Rev.* **2014**, *114*, 8613-8661.

(4) (a) T. Seiser; G. Cathomen; N. Cramer, *Synlett.* **2010**, 1699-1703; (b) T. Seiser; N. Cramer, *Chem-eur. J.* **2010**, *16*, 3383-3391; (c) T. Seiser; N. Cramer, *J. Am. Chem. Soc.* **2010**, *132*, 5340-5341; (d) T. Seiser; N. Cramer, *Chimia* **2010**, *64*, 153-156; (e) T. Seiser; T. Saget; D. N. Tran; N. Cramer, *Angew. Chem. Int. Ed.* **2011**, *50*, 7740-7752; (f) N. Cramer; T. Seiser, *Synlett.* **2011**, 449-460; (g) T. Seiser; N. Cramer, *Org. Biomol. Chem.* **2009**, *7*, 2835-2840; (h) T. Seiser; O. A. Roth; N. Cramer, *Angew. Chem. Int. Ed.* **2009**, *48*, 6320-6323; (i) N. Ishida; Y. Nakanishi; M. Murakami, *Angew. Chem. Int. Ed.* **2013**, *52*, 11875-11878; (j) L. Souillart; N. Cramer, *Chem. Sci.* **2014**, *5*, 837-840; (k) N. Ishida; Y. Shimamoto; T. Yano; M. Murakami, *J. Am. Chem. Soc.* **2013**, *135*, 19103-19106.

(5) (a) L. T. Liu; N. Ishida; M. Murakami, *Angew. Chem. Int. Ed.* **2012**, *51*, 2485-2488; (b) L. Souillart; E. Parker; N. Cramer, *Angew. Chem. Int. Ed.* **2014**, *53*, 3001-3005; (c) T. Xu; H. M. Ko; N. A. Savage; G. B. Dong, *J. Am. Chem. Soc.* **2012**, *134*, 20005-20008; (d) A. M. Dreis; C. J. Douglas, *J. Am. Chem. Soc.* **2009**, *131*, 412-413; (e) Y. Nakao; S. Ebata; A. Yada; T. Hiyama; M. Ikawa; S. Ogoshi, *J. Am. Chem. Soc.* **2008**, *130*, 12874-12875; (f) M. P. Watson; E. N. Jacobsen, *J. Am. Chem. Soc.* **2008**, *130*, 12594-12595.

(6) (a) T. Kondo; Y. Kaneko; Y. Taguchi; A. Nakamura; T. Okada; M. Shiotsuki; Y. Ura; K. Wada; T. Mitsudo, *J. Am. Chem. Soc.* **2002**, *124*, 6824-6825; (b) M. H. Shaw; E. Y. Melikhova; D. P. Kloer; W. G.

Whittingham; J. F. Bower, *J. Am. Chem. Soc.* **2013**, *135*, 4992-4995.
(7) (a) J. J. Eisch; R. Sanchez, *J. Organomet. Chem.* **1985**, *296*, C27-C31; (b) T. Matsuda; T. Tsuboi; M. Murakami, *J. Am. Chem. Soc.* **2007**, *129*, 12596-12597.
(8) (a) J. Barluenga; C. Valdes, *Angew. Chem. Int. Ed.* **2011**, *50*, 7486-7500; (b) Z. Shao; H. Zhang, *Chem. Soc. Rev.* **2012**, *41*, 560-572; (c) Q. Xiao; Y. Zhang; J. B. Wang, *Accounts. Chem. Res.* **2013**, *46*, 236-247; (d) Y. T. Tsoi; Z. Y. Zhou; W. Y. Yu, *Org. Lett.* **2011**, *13*, 5370-5373; (e) L. Ding; N. Ishida; M. Murakami; K. Morokuma, *J. Am. Chem. Soc.* **2014**, *136*, 169-178; (f) Y. Li; Z. Lin, *J. Org. Chem.* **2013**, *78*, 11357-11365.
(9) N. Ishida; S. Sawano; Y. Masuda; M. Murakami, *J. Am. Chem. Soc.* **2012**, *134*, 17502-17504.
(10) Y. Xia; Z. Liu; Z. Liu; R. Ge; F. Ye; M. Hossain; Y. Zhang; J. Wang, *J. Am. Chem. Soc.* **2014**, *136*, 3013-3015.
(11) A. Yada; S. Fujita; M. Murakami, *J. Am. Chem. Soc.* **2014**, *136*, 7217-7220.
(12) (a) A. Vigalok; D. Milstein, *Organometallics* **2000**, *19*, 2341-2345; (b) R. Cohen; B. Rybtchinski; M. Gandelman; H. Rozenberg; J. M. L. Martin; D. Milstein, *J. Am. Chem. Soc.* **2003**, *125*, 6532-6546.
(13) A. J. C. Walters; O. Troeppner; I. Ivanovic-Burmazovic; C. Tejel; M. P. del Rio; J. N. H. Reek; B. Bruin, *Angew. Chem. Int. Ed.* **2012**, *51*, 5157-5161.
(14) P. Tian; H. Q. Dong; G. Q. Lin, *Acs Catal.* **2012**, *2*, 95-119.
(15) (a) D. H. Wei; M. S. Tang, *J. Phys. Chem. A* **2009**, *113*, 11035-11041; (b) W. J. Zhang; Y. Y. Zhu; D. H. Wei; M. S. Tang, *J. Comput. Chem.* **2012**, *33*, 715-722.
(16) (a) Z. Y. Li; D. H. Wei; Y. Wang; Y. Y. Zhu; M. S. Tang, *J. Org. Chem.* **2014**, *79*, 3069-3078; (b) Y. Wang; D. H. Wei; Z. Y. Li; Y. Y. Zhu; M. S. Tang, *J. Phys. Chem. A* **2014**, *118*, 4288-4300; (c) Y. Qiao; K. L. Han; C. G. Zhan, *Org. Biomol. Chem.* **2014**, *12*, 2214-2227; (d) D. M. Li; Y. Wang; C. L. Yang; K. L. Han, *Dalton Trans.* **2009**, 291-297; (e) M. M. Zhang; D. H. Wei; Y. Wang; S. J. Li; J. F. Liu; Y. Y. Zhu; M. S. Tang, *Org. Biomol. Chem.* **2014**, *12*, 6374-6383.
(17) (a) W. J. Chen; Z. Y. Lin, *Dalton Trans.* **2014**, *43*, 11138-11144; (b) X. Hong; B. M. Trost; K. N. Houk, *J. Am. Chem. Soc.* **2013**, *135*, 6588-6600; (c) X. F. Xu; P. Liu; A. Lesser; L. E. Sirois; P. A. Wender; K. N. Houk, *J. Am. Chem. Soc.* **2012**, *134*, 11012-11025; (d) X. F. Xu; P. Liu; X. Z. Shu; W. P. Tang; K. N. Houk, *J. Am. Chem. Soc.* **2013**, *135*, 9271-9274; (e) X. Hong; P. Liu; K. N. Houk, *J. Am. Chem. Soc.* **2013**, *135*, 1456-1462; (f) M. H. Baik; E. W. Baum; M. C. Burland; P. A. Evans, *J. Am. Chem. Soc.* **2005**, *127*, 1602-1603; (g) L. W. Chung; O. Wiest; Y. D. Wu, *J. Org. Chem.* **2008**, *73*, 2649-2655; (h) W. H. Pitcock; R. L. Lord; M. H. Baik, *J. Am. Chem. Soc.* **2008**, *130*, 5821-5830; (i) H. Wang; J. R. Sawyer; P. A. Evans; M. H. Baik, *Angew. Chem. Int. Ed.* **2008**, *47*, 342-345; (j) Y. F. Yang; T. Shi; X. H. Zhang; Z. X. Tang; Z. Y. Wen; J. M. Quan; Y. D. Wu, *Org. Biomol. Chem.* **2011**, *9*, 5845-5855; (k) M. H. Baik; S. Mazumder; P. Ricci; J. R. Sawyer; Y. G. Song; H. J. Wang; P. A. Evans, *J. Am. Chem. Soc.* **2011**, *133*, 7621-7623; (l) L. Jiao; M. Lin; Z. X. Yu, *J. Am. Chem. Soc.* **2011**, *133*, 447-461; (m) M. Lin; G. Y. Kang; Y. A. Guo; Z. X. Yu, *J. Am. Chem. Soc.* **2012**, *134*, 398-405; (n) S. Mazumder; D. J. Shang; D. E. Negru; M. H. Baik; P. A. Evans, *J. Am. Chem. Soc.* **2012**, *134*, 20569-20572; (o) Z. J. Li; V. Boyarskikh; J. H. Hansen; J. Autschbach; D. G. Musaev; H. M. L. Davies, *J. Am. Chem. Soc.* **2012**, *134*, 15497-15504; (p) Q. Zhang; H. Z. Yu; Y. T. Li; L. Liu; Y. Huang; Y. Fu, *Dalton Trans.* **2013**, *42*, 4175-4184; (q) X. F. Lin; Y. H. Lv; Y. Y. Qu; G. D. Zhang; Y. Y. Xi; D. L. Phillips; C. G. Liu, *Phys. Chem. Chem. Phys.* **2013**, *15*, 20120-20133; (r) Y. Han; M. Sun; W. Li; J. Zhang, *Phys. Chem. Chem. Phys.* **2015**, *17*, 7720-7730; (s) S. Zhang; L. Huang; L. Sun, *Dalton Trans.* **2015**, *44*, 4613-4622; (t) L. Cheng; J. Li; Q. C. Zhang; L. S. Ma; J. C. Yang, *Dalton Trans.* **2015**, *DOI: 10.1039/C4DT03051F*; (u) M. Quan; G. Q. Yang; F. Xie; I. D. Gridnev; W. B. Zhang, *Org. Chem. Front.*

2015, *2*, 398-402; (v) L. Zhang; D. C. Fang, *J. Org. Chem.* **2013**, *78*, 2405-2412; (w) B. Lian; L. Zhang; G. A. Chass; D. C. Fang, *J. Org. Chem.* **2013**, *78*, 8376-8385; (x) Y. M. Xing; L. Zhang; D. C. Fang, *Organometallics* **2015**, *34*, 770-777.

(18) (a) D. H. Wei; B. L. Lei; M. S. Tang; C. G. Zhan, *J. Am. Chem. Soc.* **2012**, *134*, 10436-10450; (b) D. M. Li; X. Q. Huang; K. L. Han; C. G. Zhan, *J. Am. Chem. Soc.* **2011**, *133*, 7416-7427; (c) D. M. Li; Y. Wang; K. L. Han, *Coordin. Chem. Rev.* **2012**, *256*, 1137-1150.

(19) G. W. S. M. J. T. Frisch, H. B.; Scuseria, G. E.; Robb, M. A.; Cheeseman, J. R.; Scalmani, G.; Barone, V.; Mennucci, B.; Petersson, G. A.; Nakatsuji, H.; Caricato, M.; Li, X.; Hratchian, H. P.; Izmaylov, A. F.; Bloino, J.; Zheng, G.; Sonnenberg, J. L.; Hada, M.; Ehara, M.; Toyota, K.; Fukuda, R.; Hasegawa, J.; Ishida, M.; Nakajima, T.; Honda, Y.; Kitao, O.; Nakai, H.; Vreven, T.; Montgomery, Jr., J. A.; Peralta, J. E.; Ogliaro, F.; Bearpark, M.; Heyd, J. J.; Brothers, E.; Kudin, K. N.; Staroverov, V. N.; Kobayashi, R.; Normand, J.; Raghavachari, K.; Rendell, A.; Burant, J. C.; Iyengar, S. S.; Tomasi, J.; Cossi, M.; Rega, N.; Millam, J. M.; Klene, M.; Knox, J. E.; Cross, J. B.; Bakken, V.; Adamo, C.; Jaramillo, J.; Gomperts, R.; Stratmann, R. E.; Yazyev, O.; Austin, A. J.; Cammi, R.; Pomelli, C.; Ochterski, J. W.; Martin, R. L.; Morokuma, K.; Zakrzewski, V. G.; Voth, G. A.; Salvador, P.; Dannenberg, J. J.; Dapprich, S.; Daniels, A. D.; Farkas, Ö.; Foresman, J. B.; Ortiz, J. V.; Cioslowski, J.; Fox, D. J., Gaussian 09, Revision C.01; Gaussian, Inc.: Wallingford, CT, 2010.

(20) (a) S. Miehlich. B., A., Stoll, H., Preuss, H., *Chem. Phys. Lett* **1989**, *157*, 200-206; (b) C. T. Lee, Yang, W. T., Parr. R. G., *Phys. Rev. B* **1988**, *37*, 785-789; (c) A. D. Becke, *J. Chem. Phys.* **1993**, *98*, 5648-5652.

(21) (a) M. Cossi; N. Rega; G. Scalmani; V. Barone, *J. Comput. Chem.* **2003**, *24*, 669-681; (b) M. C. Vincenzo Barone, *J. Phys. Chem. A* **1998**, *102*, 1995-2001.

(22) (a) C. Gonzalez, Schlegel, H. B., *J. Chem. Phys.* **1989**, *90*, 2154-2161; (b) C. Gonzalez, Schlegel, H. B., *J. Phys. Chem.* **1990**, *94*, 5523-5527.

(23) C. Y. Legault, *CYLview, 1.0b; Université de Sherbrooke, 2009 (http://www.cylview.org)*

(24) K. N. Houk, *Abstr. Pap. Am. Chem. Soc.* **2012**, *243*.

(25) (a) X. Hong, *J. Am. Chem. Soc.* **2014**, *136*, 17273; (b) A. Kina; H. Iwamura; T. Hayashi, *J. Am. Chem. Soc.* **2006**, *128*, 3904-3905.

(26) (a) C. F. Matta; R. F. W. Bader, *Proteins* **2003**, *52*, 360-399; (b) R. F. W. Bader; J. Hernandez-Trujillo; F. Cortes-Guzman, *J. Comput. Chem.* **2007**, *28*, 4-14; (c) R. F. W. Bader; C. F. Matta, *Found. Chem.* **2013**, *15*, 253-276.

(27) F. W. J. P. Foster, *J. Am. Chem. Soc.* **1980**, *102*, 7211-7218.

(28) (a) E. R. Johnson; S. Keinan; P. Mori-Sanchez; J. Contreras-Garcia; A. J. Cohen; W. T. Yang, *J. Am. Chem. Soc.* **2010**, *132*, 6498-6506; (b) J. Contreras-Garcia; E. R. Johnson; S. Keinan; R. Chaudret; J. P. Piquemal; D. N. Beratan; W. T. Yang, *J. Chem. Theory Comput.* **2011**, *7*, 625-632.